Astronomy
&
Astrophysics

Abundant molecular gas in tidal dwarf galaxies:
On-going galaxy formation

J. Braine[1], P.-A. Duc[2], U. Lisenfeld[3], V. Charmandaris[4], O. Vallejo[1], S. Leon[5], and E. Brinks[6]

[1] Observatoire de Bordeaux, UMR 5804, CNRS/INSU, BP 89, 33270 Floirac, France
[2] CNRS URA 2052 and CEA/DSM/DAPNIA, Service d'astrophysique, Saclay, 91191 Gif sur Yvette Cedex, France
[3] Institut de Radioastronomie Millimétrique, Avenida Divina Pastora 7, NC 18012 Granada, Spain
[4] Cornell University, Astronomy Department, Ithaca, NY 14853, USA
[5] ASIAA, Academia Sinica, PO Box 1-87, Nanking, Taipei 115, Taiwan
[6] Departamento de Astronomía, Universidad de Guanajuato, Apdo. Postal 144, Guanajuato, Mexico

Abstract. We investigate the process of galaxy formation as can be observed in the only currently forming galaxies – the so-called Tidal Dwarf Galaxies, hereafter TDGs – through observations of the molecular gas detected via its CO (Carbon Monoxide) emission. These objects are formed of material torn off of the outer parts of a spiral disk due to tidal forces in a collision between two massive galaxies. Molecular gas is a key element in the galaxy formation process, providing the link between a cloud of gas and a bona fide galaxy. We have detected CO in 8 TDGs (two of them have already been published in Braine et al. 2000, hereafter Paper I), with an overall detection rate of 80%, showing that molecular gas is abundant in TDGs, up to a few 10^8 $M_\odot$. The CO emission coincides both spatially and kinematically with the HI emission, indicating that the molecular gas forms from the atomic hydrogen where the HI column density is high. A possible trend of more evolved TDGs having greater molecular gas masses is observed, in accord with the transformation of HI into H_2. Although TDGs share many of the properties of small irregulars, their CO luminosity is much greater (factor ~100) than that of standard dwarf galaxies of comparable luminosity. This is most likely a consequence of the higher metallicity ($\gtrsim 1/3$ solar) of TDGs which makes CO a good tracer of molecular gas. This allows us to study star formation in environments ordinarily inaccessible due to the extreme difficulty of measuring the molecular gas mass. The star formation efficiency, measured by the CO luminosity per Hα flux, is the same in TDGs and full-sized spirals. CO is likely the best tracer of the dynamics of these objects because some fraction of the HI near the TDGs may be part of the tidal tail and not bound to the TDG. Although uncertainties are large for individual objects, as the geometry is unknown, our sample is now of eight detected objects and we find that the "dynamical" masses of TDGs, estimated from the CO line widths, seem not to be greater than the "visible" masses (HI + H_2 + a stellar component). Although higher spatial resolution CO (and HI) observations would help reduce the uncertainties, we find that TDGs require no dark matter, which would make them the only galaxy-sized systems where this is the case. Dark matter in spirals should then be in a halo and not a rotating disk. Most dwarf galaxies are dark matter-rich, implying that they are *not* of tidal origin. We provide strong evidence that TDGs are self-gravitating entities, implying that we are witnessing the ensemble of processes in galaxy formation: concentration of large amounts of gas in a bound object, condensation of the gas, which is atomic at this point, to form molecular gas and the subsequent star formation from the dense molecular component.

Key words. stars: formation – galaxies: evolution – galaxies: formation – galaxies: interactions – galaxies: ISM – cosmology: dark matter

1. Introduction

Tidal Dwarf Galaxies (TDGs) are small galaxies which are currently forming from material ejected from the disks of spiral galaxies through collisions. They allow us to ob-

serve processes – galaxy formation and evolution – similar to what occurred in the very early universe but in very local objects. As a consequence, they can be studied with a sensitivity and a resolution unimaginable for high-redshift sources. Because galactic collisions can be well reproduced through numerical simulations, it is possible to obtain good age estimates for the individual systems (e.g.

Duc et al. 2000). The formation of TDGs is not exactly the same as what happened during the major episode of galaxy formation in that the material which TDGs are made from is "recycled", as it was already part of a galaxy. In particular, the presence of metals, both in gas and as dust, facilitates the cooling of the gas and the formation of H_2 molecules. Nevertheless, both for TDGs and in the early universe, the galaxy formation process involves clouds of atomic hydrogen (HI) gas gradually condensing through their own gravity, becoming progressively denser, fragmenting, forming molecular gas from the atomic material, and then forming stars. How this occurs in detail at high redshift is unknown and is one reason for studying TDGs.

Perhaps the least well known of these processes is the transformation of atomic into molecular gas because of the difficulty of observing molecular gas in very low-metallicity environments (e.g. Taylor et al. 1998). Because TDGs condense from matter taken from the outer disks of spiral galaxies, the metallicity of the gas they contain is typically only slightly subsolar as opposed to highly subsolar for small dwarf galaxies (Duc et al. 2000). The metallicity dependent CO lines can thus be used as a probe of the molecular gas content as in spiral galaxies.

Using the word "Galaxy" implies belief that they are kinematically distinct self-gravitating entities (Duc et al. 2000) and indeed this has remained one of the major questions about these small systems. The detection of large quantities of molecular gas, formed in all likelihood from the conversion of HI into H_2, indicates that the central regions are gravitationally bound entities, dynamically distinct from the tidal tails (Duc & Mirabel 1998). Not all of the material in the vicinity is necessarily bound to the condensing region, however, nor are we sure that TDGs will not fall back onto the parent merger at some time. The CO belongs to the bound regions and as such could be an excellent tracer of total (dynamical) mass, either through a rotation curve or through the size and linewidth. TDGs form at the ends of tidal tails and as such are made of the parts of spiral disks with the most angular momentum – the exterior. This is also where the need for dark matter in spirals is greatest. If dark matter in spirals is in a halo, then little of it should be projected out, and into TDGs, due to the lack of angular momentum (Barnes & Hernquist 1992). This should make TDGs the only known galaxies without significant quantities of dark matter. On the other hand, if TDGs are shown to contain dark matter as other dwarf galaxies, then the unseen material presumably lies in the outer disks of spirals, not following conventional cold dark matter (CDM) wisdom (e.g. Peebles 1982; Blumenthal et al. 1984).

TDGs, and dwarf galaxies in general, contain lots of gas, a highly varying amount of star formation, and usually an older stellar component (Weilbacher et al. 2000). They are found at the ends of tidal tails which can reach 100 kpc from the nuclei of the parent galaxies. Hα emission, showing that young stars are present, is typically found at or very near the peak HI column density. The first detections of molecular gas in TDGs (Braine et al. 2000, hereafter Paper I) showed that there was a tight link between the CO and the HI. In this paper, we present further detections of molecular gas, via the CO lines, in tidal dwarf galaxies. Table 1 lists the systems we have observed along with the TDG coordinates.

The study of TDGs influences three areas of astronomy: star formation, dark matter, and galaxy formation. We adopt this as the layout for this article. After presenting the observations (Sect. 2), we explore the unique possibility provided by TDGs to study star formation in the dwarf galaxy environment, due to the metallicity which allows us to detect molecular lines as in spirals (Sect. 3). The following section describes the phase of collapse and the ensuing transformation of atomic into molecular gas. The link between dynamical and "visible" masses, the need for dark matter, and the consequences are dealt with in Sect. 5. TDGs are not the only systems where molecular gas is detected in unusual places and we present these cases briefly in Appendix A. Appendix B provides new data for the central galaxies.

2. Observations and results

Our sample consists of interacting systems for which an extensive set of optical and radio (HI) data already exist in the literature. They are listed in Table 1 and their properties presented in Table 2. Further optical observations, some of which are still unpublished, are described in Table 3.

During observing runs in June and November 1999, and March and September 2000 we observed the CO(1–0) and CO(2–1) lines at 115 and 230 GHz with the 30 meter antenna on Pico Veleta (Spain) run by the Institut de Radio Astronomie Millimétrique (IRAM). Dual polarization receivers were used at both frequencies with, typically, the 512×1 MHz filter backends on the CO(1–0) line and the autocorrelator for the CO(2–1). Pointing was monitored on nearby quasars every 60–90 min and found to be accurate to $\approx 3''$ rms. Before observing each source of interest (the TDG), we checked the frequency tuning by observing the Orion RC2 or Sagitarius B2 for which observations and line identifications are available (Turner 1989; Sutton et al. 1985) over the entire frequency range. System temperatures were typically quite good, 150–200 K and 200–300 K at 115 and 230 GHz respectively on the T_a^* scale. IRAM forward (main beam) efficiencies are 0.9 (0.72) and 0.84 (0.48) at 115 and 230 GHz respectively. IRAM half-power beamsizes are $21''$ and $11''$ at 115 and 230 GHz respectively. All CO spectra and intensities are given using the main beam temperature scale.

In observations performed in a very similar way, NGC 5291 and the associated TDGs were observed at the SEST[1] 15 m telescope in July 1998; NGC 2992/3

Table 1. Coordinates, velocities, and distances ($H_0 = 75\,\mathrm{km\,s^{-1}\,Mpc^{-1}}$) of observed systems. The 4th column gives the velocity as $v_{\mathrm{opt}} = cz$ where z is the redshift. The Arp 105 and Arp 245 systems were presented in Braine et al. (2000). Stephan's Quintet is Hickson Compact Group 92 (Hickson 1982).

Source	RA	Dec	V_{opt}	Dist.	Short description
	J2000	J2000	cz, $\mathrm{km\,s^{-1}}$	Mpc	
NGC 7252W	22 20 33.6	–24 37 24	4822	64	advanced merger, spiral + spiral
NGC 4038S	12 01 25.6	–19 00 34	1660	22	early stage merger, spiral + spiral
NGC 4676N	12 46 10.5	+30 45 37	6700	90	early stage merger, spiral + spiral
NGC 5291N	13 47 20.5	–30 20 51	4128	58	collision of spiral + lenticular
NGC 5291S	13 47 23.0	–30 27 30	4660	58	
NGC 7319E	22 36 10.3	+33 57 17	6600	90	Stephan's Quintet: tail from spiral NGC 7319
NGC 2782W	09 13 48.5	+40 10 11	2553	33	advanced merger?
IC 1182E	16 05 42.0	+17 48 02	10090	135	advanced merger, spiral + spiral?
UGC 957	01 24 24.4	+03 52 57	2145	28	NGC 520 system, spiral + spiral

Table 2. Sample of Tidal Dwarf Galaxies and related objects. CO observations (and thus molecular gas masses) are from this paper except for Arp 245N and Arp 105S which were presented in Paper I. Except where noted, the CO data are in the CO(1–0) line. We have attempted to estimate the HI column density (Col. 6) over an area similar to that of the CO beam. Data for NGC 4676N includes both positions observed (I_{CO} and N_{HI} are averages, S_{CO} and M_{mol} are total).

System	TDG	I_{CO}	S_{CO}	M_{mol}	N_{HI}	$L_{\mathrm{H\alpha}}$	metallicity
		$\mathrm{K\,km\,s^{-1}}$	$\mathrm{Jy\,km\,s^{-1}}$	$10^8\,M_\odot$	$10^{20}\,\mathrm{cm^{-2}}$	$10^{39}\,\mathrm{erg\,s^{-1}}$	$12+\log(\mathrm{O/H})$
Arp 245	Arp 245N	$1.3 \pm 0.1, 2.0 \pm 0.5^a$	6.2^b	$\sim1.5^{(1)}$	$23^{(2)}$	$7.4^{(2)}$	$8.6^{(2)}$
Arp 105	Arp 105S	0.3 ± 0.05	1.5	$2.2^{(1)}$	$3.2^{(3)}$	10–$20^{(4)}$	$8.4^{(4)}$
NGC 4676	NGC 4676N	0.13 ± 0.02	1.2	1.1	$9.5^{(5)}$	10–$20^{(6)}$	
NGC 7252	NGC 7252W	0.27 ± 0.05^a	1.3	0.2	$\gtrsim5^{(7)}$	$1.0^{(8)}$	$8.6^{(8)}$
NGC 4038	NGC 4038W	0.2 ± 0.06^a	1.0	0.02	$\sim10^{(9)}$	$1.7^{(10)}$	$8.4^{(10)}$
NGC 2782	NGC 2782W	$\lesssim0.1$	$\lesssim0.5$	$\lesssim0.06$	$\gtrsim10^{(11)}$		
IC 1182	IC 1182E	$\lesssim0.06$	$\lesssim0.27$	$\lesssim0.5$	$\sim9^{(12)}$		$8.4^{(13)}$
NGC 5291	NGC 5291N	0.3 ± 0.07	5	1.9	$13^{(14)}$	$8.9^{(15)}$	$8.4^{(15)}$
NGC 5291	NGC 5291S	0.4 ± 0.1	8	2.9	$7^{(14)}$	$4.4^{(15)}$	$8.5^{(15)}$
Stephan's Quintet	NGC 7319E	1.1 ± 0.06	5.2	4.5	$\gtrsim7^{(16)}$	$13.6^{(17)}$	
NGC 520	UGC 957	$\lesssim0.07$	$\lesssim0.33$	$\lesssim0.03$	$2.5^{(18)}$		

^{a} CO(2–1) measurement.
^{b} Extended source, central flux only.
In addition to this paper, references are: 1 = Paper I; 2 = Duc et al. (2000); 3 = Duc et al. (1997); 4 = Duc & Mirabel (1994), Hα flux is estimated from the long slit data; 5 = Hibbard, priv. comm.; 6 = estimated from Hibbard & van Gorkom (1996); 7 = measured from Hibbard et al. (1994) HI observations, expressed as lower limit because CO beam is smaller; 8 = Duc (1995); 9 = van der Hulst (1979), Hibbard, priv. comm.; 10 = Mirabel et al. (1992); 11 = Smith (1994), expressed as lower limit because CO beam is smaller than the rectangle for which the average column density is given; 12 = Dickey (1997), where IC 1182E is called ce-061; 13 = estimated from spectrum in Bothun et al. (1981); 14 = Malphrus et al. (1997), estimated for SEST CO(1–0) resolution; 15 = Duc & Mirabel (1998); 16 = Shostak et al. (1984), expressed as lower limit because CO beam is much smaller; 17 = Xu et al. (1999), corrected for NII contamination but not extinction; 18 = estimated from Hibbard & van Gorkom (1996) Fig. 16.

(Arp 245) was observed at the SEST in Nov. 1999. Acousto-optical spectrometers were used as backends for both the CO(2–1) and CO(1–0) transitions. SEST beamsizes are respectively $43''$ and $22''$ at 115 and 230 GHz. Pointing was found to be reliable to $\approx4''$ rms and beam efficiencies are similar to those at IRAM.

The data reduction was simple. Spectra were summed and a very small continuum level, corresponding to the av-

erage difference between the atmospheric emission in the ON and OFF positions, was subtracted. For NGC 5291N and NGC 4676N CO(2–1) a first order (i.e. linear) baseline was subtracted.

CO detections were obtained for the NGC 7252 West (hereafter NGC 7252W), NGC 4676 North (hereafter NGC 4676N), NGC 5291 North and NGC 5291 South (hereafter NGC 5291N and NGC 5291S), Stephan's
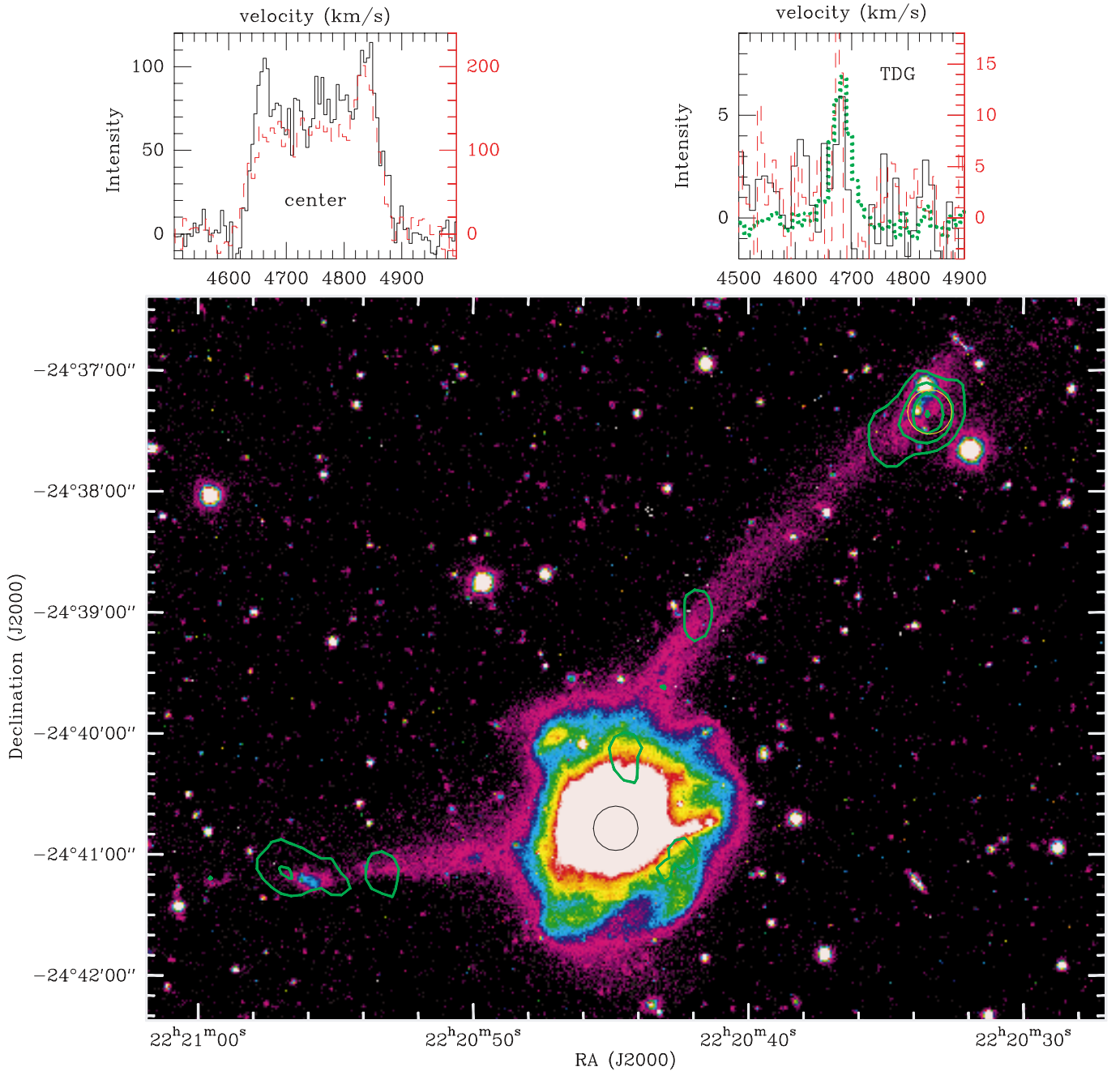
Fig. 1. *V*-band image of the NGC 7252 "Atoms For Peace" system with two tidal dwarfs, NGC 7252W and NGC 7252E, the latter of which was not observed in CO. The image is saturated to show the stars in the tidal tails. The green contours represent HI column densities (Hibbard & van Gorkom 1996) of 2, 3, 4, 5 $\times 10^{20}$ cm^{-2} at $27'' \times 16''$ resolution. Circles show the positions observed in CO; the size of the circle is that of the CO(1–0) beam. Above the image the spectra of the Western TDG, NGC 7252W, and the center of the merger are shown and color coded as follows: HI as thick dotted green, CO(1–0) as black and CO(2–1) as dashed red. The velocities are in km s^{-1} and the left vertical scale gives the intensity in mJy per beam for the HI and mK for the CO(1–0). The right vertical scale indicates the CO(2–1) line strength in mK. CO observations are presented on the main beam temperature scale.

Quintet source "B" (hereafter NGC 7319E), and very probably the NGC 4038/9 South ("The Antennae", hereafter NGC4038S) TDGs. Figures 1–7 show optical images of these galaxies with contours showing the HI emission. All coordinates are given in the J2000 coordinate system. No detection was obtained of the tidal dwarf associated with the IC 1182 system. The western

tail of the NGC 2782 (Arp 215) system was also observed with no CO detection, confirming the Smith et al. (1999) non-detection. The western HI tail of NGC 2782 has presumably not had time to condense into H$_2$ and for star formation to begin (see below). UGC 957, possibly a TDG linked to the NGC 520 merger (Arp 157), was not detected in CO. The compact tidal dwarf associated with
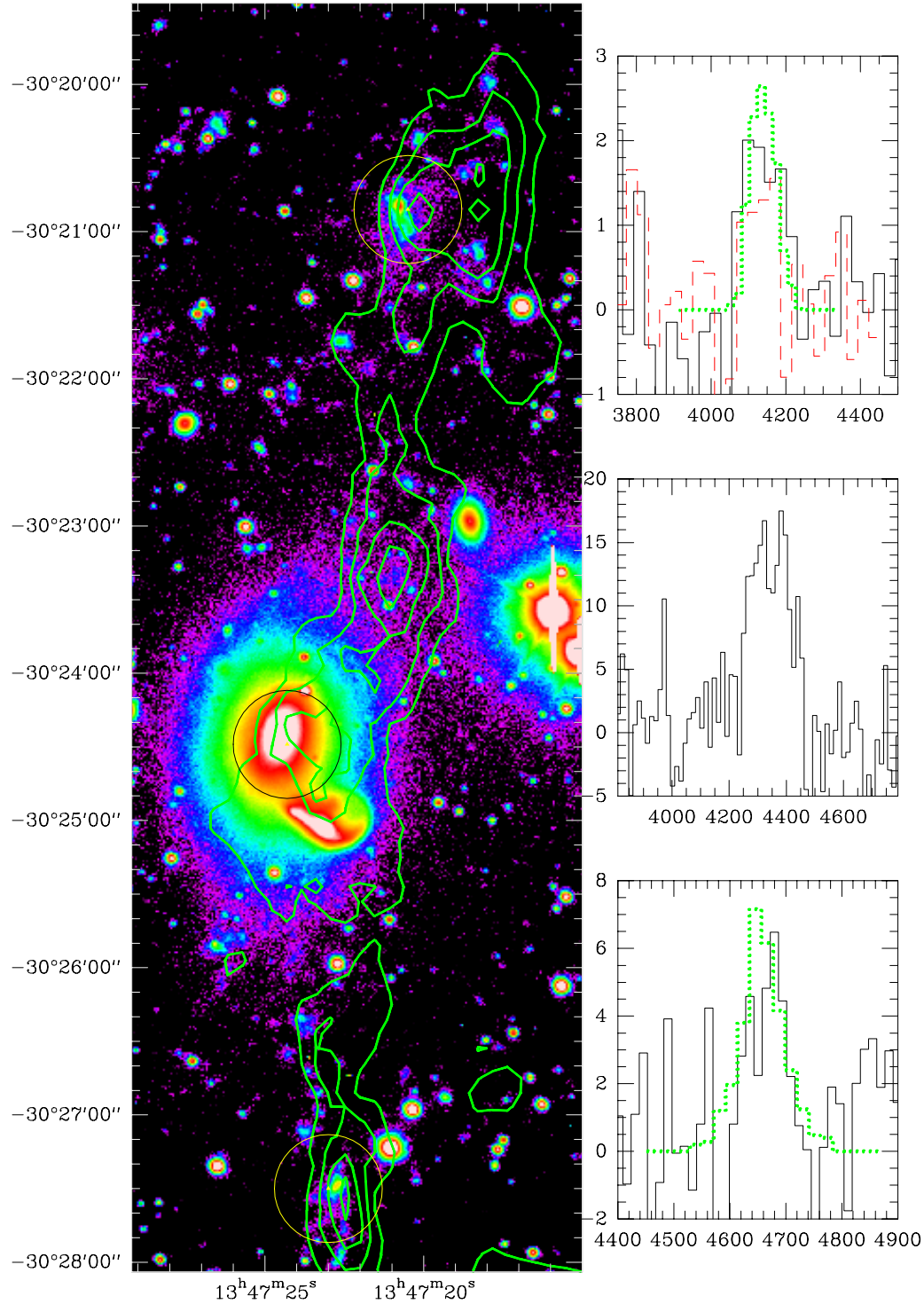
Fig. 2. The NGC 5291 system: R band image (Duc & Mirabel 1998) with HI contours (Malphrus et al. 1997) superimposed. First HI contour and contour spacing is 5×10^{20} cm^{-2}; the spatial resolution is $26'' \times 15''$. Spectrum is color coded as in Fig. 1; for the top spectrum, the left scale indicates both CO(1–0) and CO(2–1) intensity in mK. HI spectra are in arbitrary units. The circles mark the positions observed in CO and their spectra are adjacent.

the NGC 3561 (Arp 105) system, Arp105S, and the tidal dwarf of the NGC 2992/3 (Arp 245) system, Arp245N, were detected in the first run and described in Paper I. The immediate result is that almost all sources were detected in CO.

In Figs. 1–7 we present the CO spectra of the detected TDGs with the HI spectrum, when available, superimposed in order to illustrate the great similarity. The figures are color-coded such that HI, when present, is always a full green contour on the optical images and a
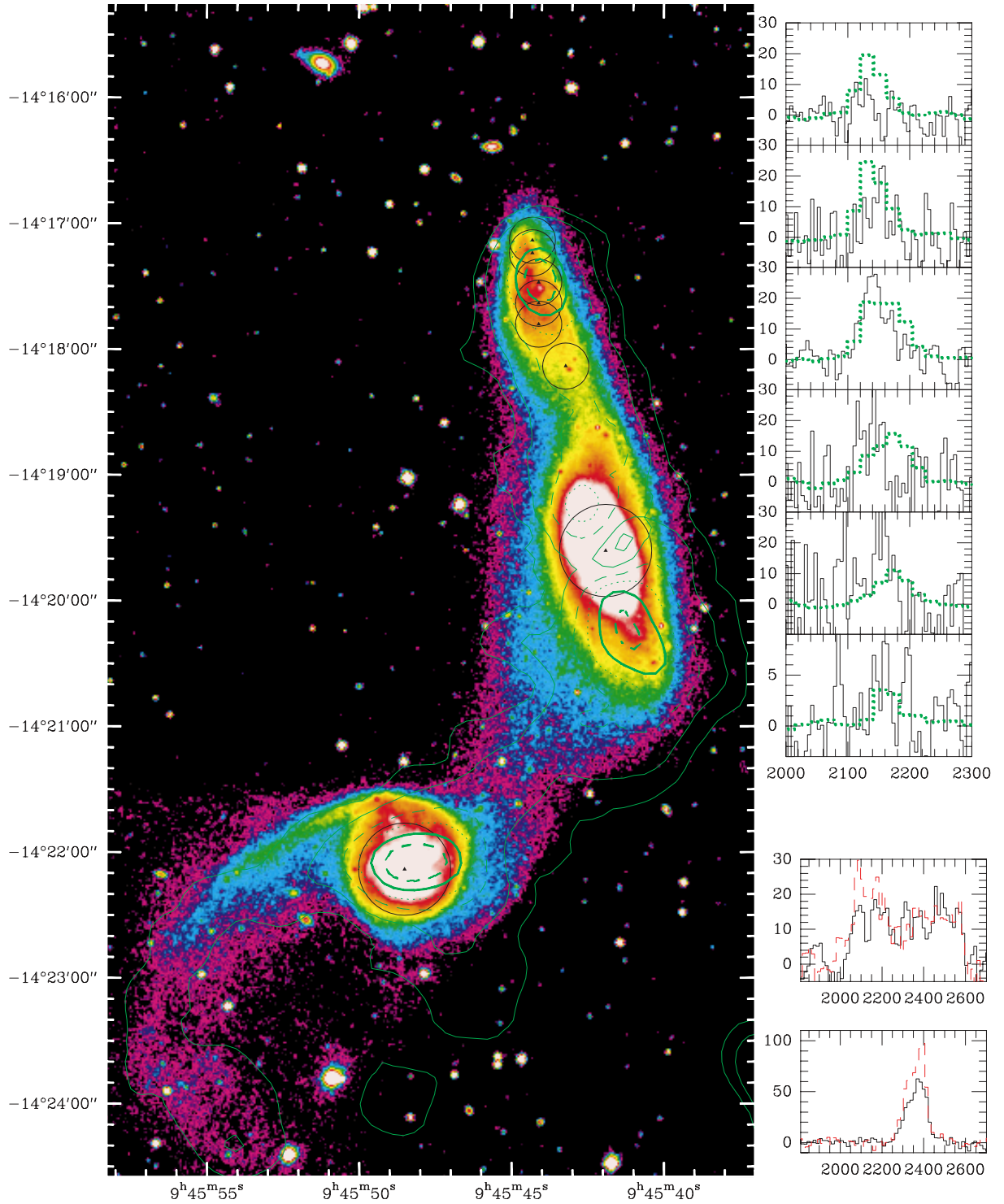
Fig. 3. The Arp 245 (NGC 2992/3) system: *V* band image with HI contours (Duc et al. 2000) superimposed in green. HI contours are 2, 4 (full), 8 (dashed), 12 (dotted), 16 (thick), and 20 (thick dashed) $\times 10^{20}$ cm^{-2}. The black circles show the CO(1–0) beamwidth, small for IRAM and large for SEST, and mark the positions observed in CO. The top six spectra are of the TDG at the positions of the circles from North to South and below are the spectra of the centers of NGC 2992 and 2993 (bottom), where the scale indicates CO(1–0) intensity in mK; HI spectra are in arbitrary units. The new CO spectra have been added to the data presented in Paper I.

thick dotted green line on the spectra, in arbitrary flux units except when specified otherwise in the figure caption. CO spectra are in milliKelvins (mK), take a full black line, and follow the left *y*-axis scale. When both CO(2–1) and CO(1–0) are present, the CO(1–0) takes a full black line and follows the left *y*-axis scale while the CO(2–1)
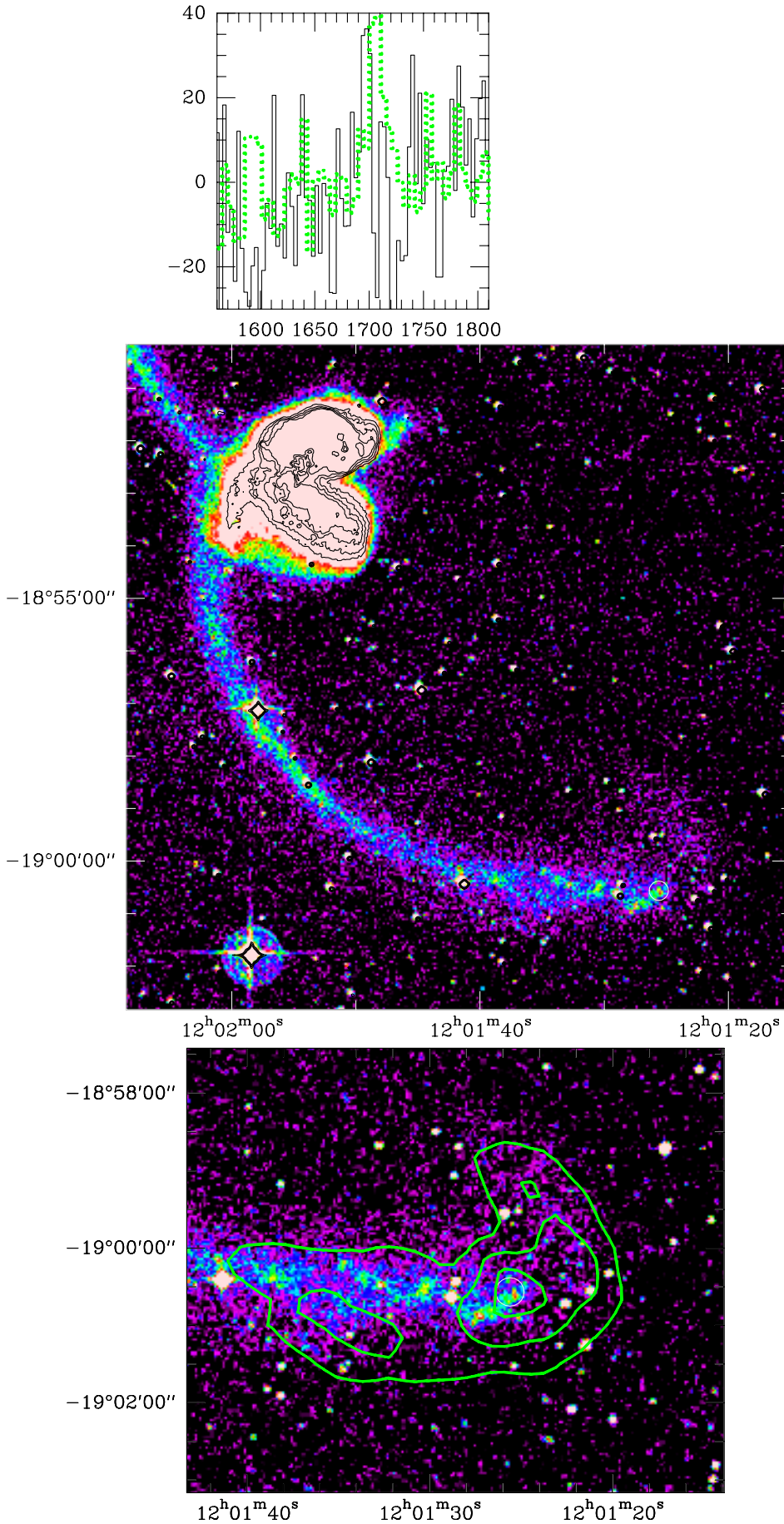
Fig. 4. UK Schmidt Digital Sky Survey image of The Antennae (NGC 4038/9). Middle panel shows overall optical view and lower panel shows a close-up of the TDG with HI (green) contours of 2, 4, and 6×10^{20} cm^{-2} at $46 \times 33''$ resolution on optical. All HI here is from Hibbard et al. (in prep); see also published HI observations by van der Hulst (1979). The circle marks the position observed in CO. The CO(2–1) spectrum (black line, left scale) and high resolution HI spectrum (dotted green, arbitrary units) are shown in the top panel. The tentative detection of a wide CO line in the TDG with a peak at $v \approx 1600$ km s^{-1} by Gao et al. (2001) is not confirmed.
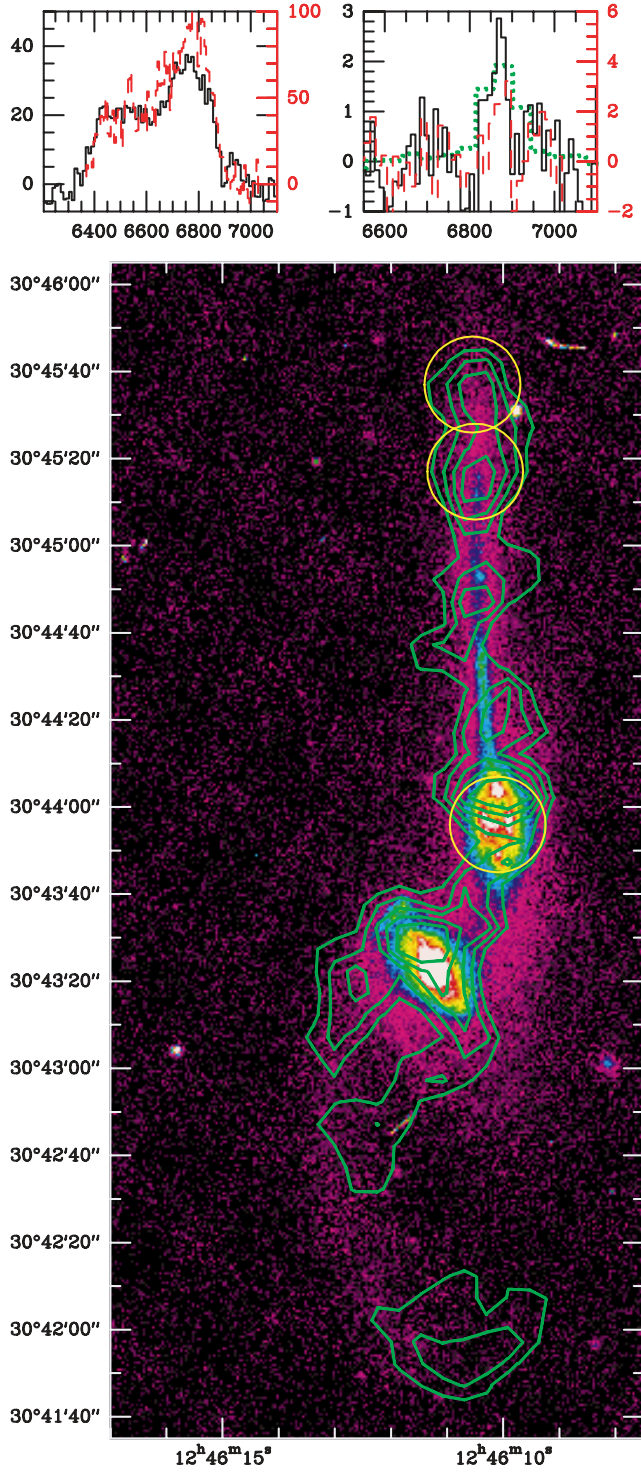
Fig. 5. The NGC 4676 "The Mice" system: R band image with green HI contours (Hibbard & van Gorkom 1996) superimposed. First HI contour and contour spacing is 2.5×10^{20} cm^{-2}; the spatial resolution is $12''$. The circles mark the positions observed in CO and the TDG spectra are at the top right and the spectra of the center of NGC 4676a (Northern spiral) at the top left. The TDG CO spectra are the sum of the two positions towards the end of the tidal tail. The CO(2–1) spectra (red, dashed) follow the red right scale and the HI spectrum is in arbitrary units.
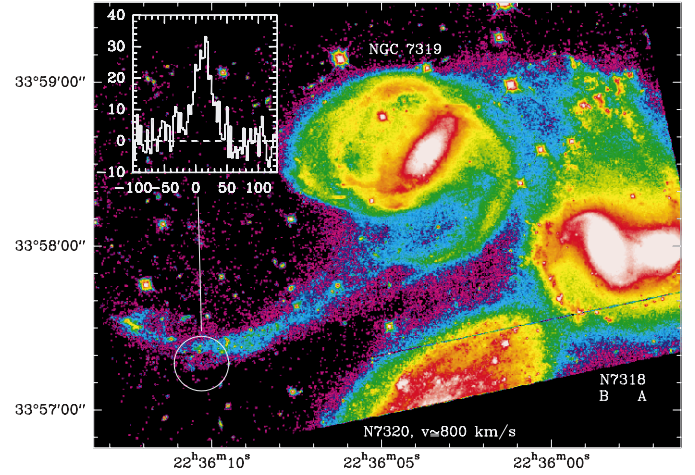
Fig. 6. Hubble Space Telescope V-band mosaic of Stephan's Quintet. Spectrum is CO(1–0) emission and the circle marks the position observed in CO, which is the HI column density peak as observed by Shostak (1984). The zero velocity corresponds to $cz = 6600$ km s^{-1}. NGC 7320 is a foreground galaxy.

Table 3. Optical observations of TDGs.

| System	Date	Tel./Instr.	Reference
Arp 245	Mar. 95	NTT/EMMI	Duc et al. (2000)
NGC 4038/9		DSS	
NGC 4676	Feb. 94	CFHT/MOS	this paper
NGC 5291	Jul. 94	NTT/EMMI	Duc & Mirabel (1998)
NGC 7252	Jul. 94	NTT/EMMI	Duc (1995)
IC 1182	Jun. 99	INT/WFC	this paper
Steph. Quint.	Jun. 99	HST/WFPC	Gallagher et al. (2001)

takes a red dashed line and follows the right y-axis scale if different from the CO(1–0). For the CO non-detections, the resulting (1σ) limits to the molecular gas mass have been calculated assuming that the CO line is as wide as the HI line and for detections and non-detections alike we used a $N(\mathrm{H}_2)/I_{\mathrm{CO}}$ factor of 2×10^{20} cm^{-2} (K km s^{-1})$^{-1}$ (e.g., Dickman et al. 1986).

Thus

$$M_{\mathrm{H}_2} = I_{\mathrm{co}} \, N(\mathrm{H}_2)/I_{\mathrm{CO}} \, D^2 \Omega \, 2m_{\mathrm{p}} \tag{1}$$

where I_{co} is the average CO line intensity expressed in K km s^{-1}, D the distance, m_{p} the proton mass, and Ω the solid angle over which the source emission is averaged. In order to obtain the total mass within the molecular gas clouds, Helium must be included such that $M_{\mathrm{mol}} = M_{\mathrm{H}_2}/f_{\mathrm{H}}$ where f_{H} is the hydrogen fraction by mass, $f_{\mathrm{H}} \sim 0.73$. For a single pointing with a Gaussian beam of full width at half power θ_{FWHM}, $\Omega = 1.13\theta_{FWHM}^2$. This is generally sufficient for our observations but becomes quite complex when attempting a comparison with data on nearby dwarf galaxies given the variety of sizes, telescopes, sampling intervals, and even temperature scales.
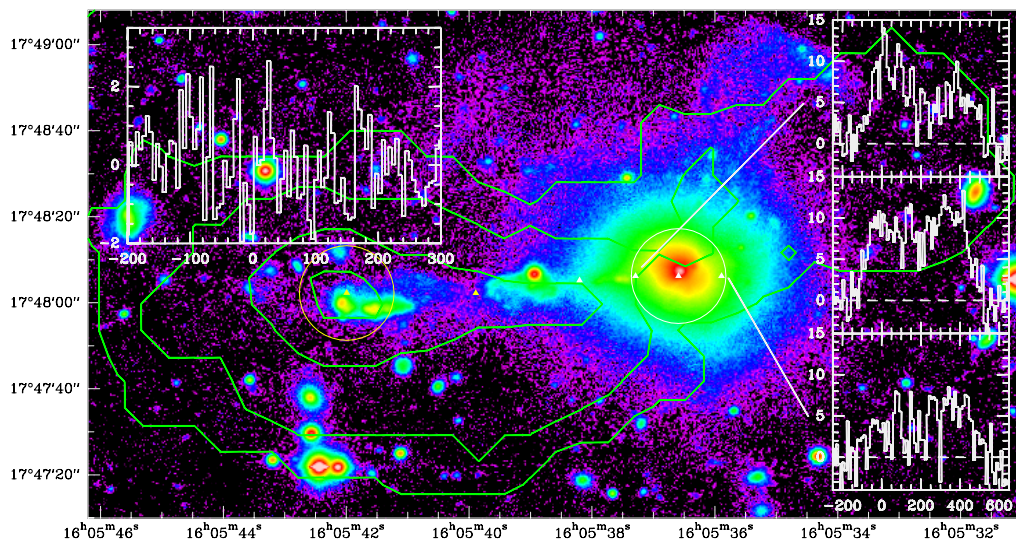
Fig. 7. R band image of the IC 1182 system. Triangles mark the positions observed and the circles show the CO(1–0) beamsize on the TDG (yellow) and merger remnant (white). Green contours indicate the HI column density (Dickey 1997) and are at 3, 4, 6, and 8×10^{20} cm^{-2}. The zero velocity corresponds to $cz = 10\,090$ km s^{-1} which is the HI velocity of the TDG. The TDG spectrum (left) is a sum of the CO(2–1) and CO(1–0) in order to get the best sensitivity possible. We treat this as a non-detection whose integrated intensity, or upper limit, is that of the vague "line", real or not, at the 1.5–2σ level at a velocity of about 20 km s^{-1}. The spectra seen to the right show the large quantity of molecular gas in the merger remnant, $M_{\rm mol} \gtrsim 5 \times 10^9$ $M_\odot$ with the CO–H$_2$ factor as used throughout this work. The gas is in rotation with the approaching (Eastern) side at the HI velocity of the TDG.

Therefore we translate all tabular data into line fluxes expressed in Jy km s^{-1}, as opposed to K km s^{-1}. In this way, one need not worry about telescope, beamsize, etc.

$$S_{\rm co} = I_{\rm co}\,\Omega\,2k\nu^2 c^{-2}\ {\rm Jy}^{-1} \qquad (2)$$

where $S_{\rm co}$ is in Jy km s^{-1}. Jy^{-1} = 10^{23} erg^{-1} s cm^2 Hz serves only to convert flux to Jy km s^{-1}. Then

$$M_{\rm mol} = D^2\,S_{\rm co}\,\frac{2m_{\rm p}}{f_{\rm H}}\,N({\rm H_2})/I_{\rm CO}\,\frac{c^2{\rm Jy}(1+z)^2}{2k\nu_0^2}. \qquad (3)$$

For D in Mpc, $N({\rm H_2})/I_{\rm CO} = 2\times10^{20}$ cm^{-2} (K km s^{-1})$^{-1}$, $\nu_0 = 115.273$ GHz (the CO(1–0) transition), and $z \approx 0$, this becomes

$$M_{\rm mol} = 1.073 \times 10^4\,D_{\rm Mpc}^2\,S_{\rm co}\ M_\odot. \qquad (4)$$

For NGC 7252W and NGC 4038S, only the CO(2–1) line was detected and so this was used to estimate the H$_2$ mass via Eq. (3) but with $\nu_0 = 230$ GHz instead of 115 GHz and assuming an intrinsic CO($\frac{2-1}{1-0}$) line ratio of 0.75. In these two sources the CO emission may well be optically thin so the molecular gas mass should be viewed as an upper limit. In NGC 4676N, the two areas (see Fig. 5) were added together, so the molecular gas mass refers to the sum of the two positions. All derived molecular gas masses are given in Table 2; they range from 2×10^6 $M_\odot$ to 4.5×10^8 $M_\odot$ with an average value of 1.8×10^8 $M_\odot$.

3. Star formation in TDGs and other dwarf galaxies

The most striking difference between TDGs and dwarf galaxies not identified as tidal is their high CO luminosities (see Fig. 8), roughly a factor 100 higher than for other dwarf galaxies of similar luminosity and star formation rate. The most important factor responsible for this difference is certainly the metallicity. As the metallicity increases, the CO lines become optically thick over a larger area and larger velocity range. Furthermore, the shielding against UV radiation due to both CO molecules and dust increases as well. For this reason, a change in metallicity is expected to have a stronger effect in a UV-bright environment (e.g. Wolfire et al. 1993; Braine et al. 1997, Sect. 7.3).

The metallicities of TDGs are (from [OIII]/Hβ line ratios) clustered around $12 + \log({\rm O/H}) = 8.5$ independent of luminosity (Duc et al. 2000) whereas non-TDGs obey a luminosity-metallicity relation (Skillman et al. 1989). Inspection of the available CO data on dwarf galaxies (see Table 4 and Taylor et al. 1998 and references therein), reveals that up to now, there are probably no real CO detections at $12 + \log({\rm O/H}) < 8$, corresponding to $M_B \gtrsim -15$ (the reported detection of CO in I Zw 36 was not confirmed by Arnault et al. 1988). The detection of several TDGs at $M_B > -15$ confirms that metallicity is indeed a key element and that luminosity is not a problem for the detection of molecular gas in TDGs as long as sufficient HI is present.

We illustrate some of the differences between TDGs, standard dwarf galaxies, and normal spirals in Fig. 8, where we show the molecular gas content derived from the CO luminosity, normalized by the star formation rate (from Hα flux) or the HI mass, as a function of luminosity and metallicity. Assuming that star formation can be traced via the Hα line, we estimate the star formation rate (SFR) as

$$SFR = 5 \times 10^{-8} L_{H\alpha}/L_\odot \ M_\odot \, \text{yr}^{-1}. \qquad (5)$$

(Hunter & Gallagher 1986). The CO/Hα flux ratio, expressed as a gas reservoir divided by star formation rate (SFR) is thus equivalent to a gas consumption time. We have assumed that close to half of the ionizing photons are lost to dust. Note that these calculations are for a Salpeter (1955) IMF ($N(m) \propto m^{-2.35}$) from 0.1 to 100 $M_\odot$. For an "average" spiral we have assumed $L_B \sim 2 \times 10^{10} \ L_{B,\odot}$ and taken the Kennicutt (1998) sample for which the average $M_{\text{mol}}/SFR = 1.5 \times 10^9$ yrs with a dispersion of a factor three. In this calculation, we have converted Kennicutt's values back to the observables (CO, Hα fluxes) and then used the $SFR/$Hα and $N(\text{H}_2)/I_{\text{CO}}$ values used in this paper.

The top panel of Fig. 8 shows that while the luminosity range of TDGs is indeed typical of dwarf galaxies, their M_{mol}/SFR ratio (equivalent to CO/Hα) is rather typical of spirals and much higher (about a factor of 100) than in dwarf galaxies. The middle panel of Fig. 8 presents the M_{mol}/SFR ratio as a function of oxygen abundance and the lower panel the $M_{\text{mol}}/M_{\text{HI}}$ ratio. TDGs appear to have more molecular gas than other dwarf galaxies even if they are of the same metallicity – the reason for this is unclear and might indicate that metallicity is not the only parameter. A higher HI surface density in TDGs that would enable molecular gas to form more easily can be excluded as a possible reason: The dwarf galaxies of Table 4 for which HI observations with sufficient resolution exist (NGC 1569, NGC 4449 and NGC 6822) show HI surface densities above 10^{21} cm^{-2} in the CO emitting region – values that are of the same order as found in the TDGs (Table 2). Some lower metallicity dwarf galaxies with no detected CO emission (Taylor et al. 1998) have very high HI column densities – e.g. DDO 210 and DDO 187 (Lo et al. 1993), Sextans A (Skillman et al. 1988), or UGC 4483 (Lo et al. 1993).

The current observations show that in TDGs, as in spiral galaxies, CO is likely a good tracer of H2 and the $N(\text{H}_2)/I_{\text{CO}}$ conversion factor does not seem to be radically different in TDGs and in spirals. The similar gas consumption times also indicate that star formation proceeds in a similar way in both spiral disks and small irregular systems as TDGs.

What can we learn about star formation from the apparent similarity of TDGs and spirals? Star formation in spiral disks can be well described by a Schmidt (1959) law ($SFR \propto (M_{\text{gas}}/\text{surface area})^n$), with a constant exponent n, when including a threshold for the onset of star formation (Kennicutt 1989). The similarity of the

SFE in TDGs and spirals provides evidence that a similar discription might be valid in TDGs. From our data we cannot say anything about the threshold for the onset of star formation because we lack spatial resolution. Kennicutt (1989) derived coherent results when applying the Toomre (1964) "Q" criterion $Q = \frac{v_{\text{gas}}\kappa}{\pi G \Sigma_{\text{gas}}}$ – where κ is the epicyclic frequency, v_{gas} the velocity dispersion of the gas, and Σ_{gas} the gas surface density – to a sample of spirals. This is, however, no definite proof that the large-scale elements in "Q" are indeed those that determine whether the star formation, which is small-scale physics, occurs. The Toomre criterion as it stands is by definition not appropriate in systems which are not clearly rotating. If the threshold for the onset of star formation would be found to be similar in spirals and in TDGs, then the "Q" criterion is likely not the appropriate controlling factor in spirals. It is, however, remarkable that the gas consumption time, the inverse of the SFE, appears not very different in spiral disks, dominated by the stellar mass, and dwarf galaxies which are dominated by the gaseous mass.
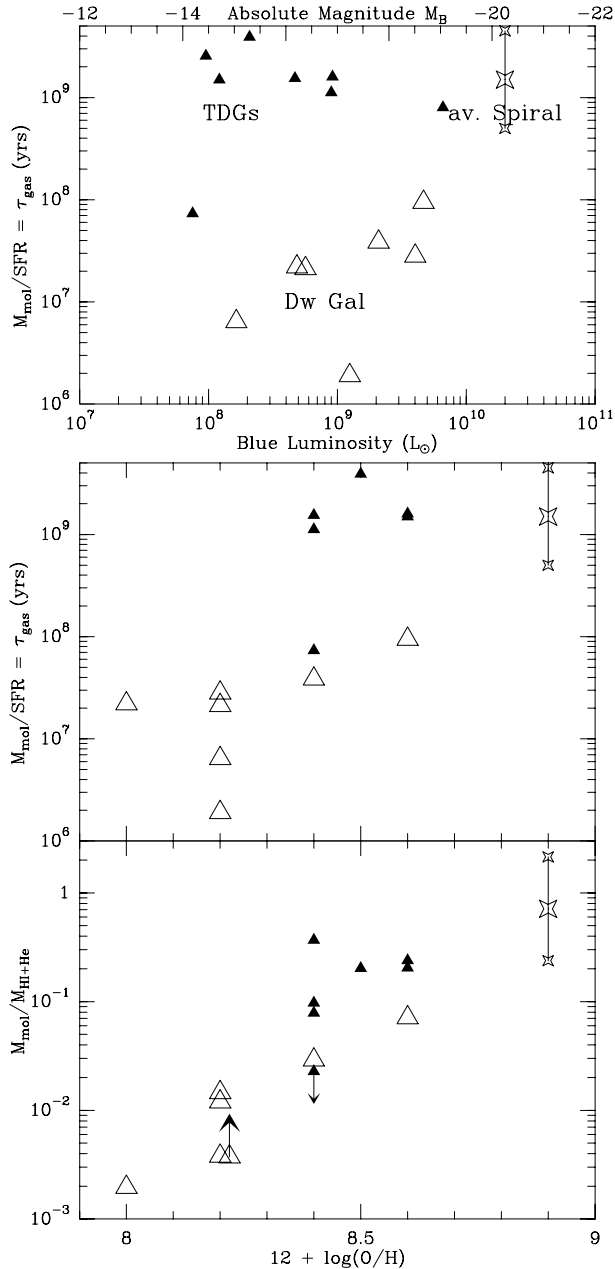
4. TDG Formation and the transformation of HI into H$_2$

We argue here that it is now possible to follow the TDG formation process from ejection to gravitational collapse to the conversion of HI into H$_2$ and the subsequent star formation.

4.1. Ejection and collapse

The formation of tidal tails from disk galaxies has been studied in detail through numerical simulations (e.g. Barnes & Hernquist 1992; Hibbard & Mihos 1995; Springel & White 1999). Every collision is unique because of the number of important parameters of the collision – spin and orbit directions, angle of disks with respect to orbit plane – as well as the unknown initial properties of the galaxies involved in the collision, which greatly vary from one system to another judging from the variety seen in non-interacting galaxies. Relatively thin tidal tails, as are typically observed in systems where TDGs are present, can be readily reproduced (Hibbard & Mihos 1995) by simulations. A fairly typical tail width is of the order of 3 kpc, or 10^{22} cm (see figures in Mihos 2001). Typical collision ages are 1–5 $\times 10^8$ yrs, setting an upper limit to the age of the forming galaxy. We must then have

$$\text{age} > t_{\text{free-fall}} = \sqrt{R^3/GM} \approx 5 \times 10^7 \ n^{-1/2} \, \text{yrs} \qquad (6)$$

where n is the gas density in cm^{-3}. We have not included the mass of stars ejected from the spiral disk, which may reduce the free-fall time slightly in some cases, but the

current stellar luminosity from TDGs is generally dominated by the new (formed in situ) population (Weilbacher et al. 2000). Although the ratio differs greatly from one TDG to another (e.g. Fig. 10), the gas masses are frequently greater than the stellar masses. Furthermore, only the gaseous component will contract and cool.

In order to form a galaxy, the relevant part of the tidal arm must then have a density of $n \gtrsim 0.1$ cm^{-3}. This coincides very well with typical column densities towards tidal dwarf galaxies, $N(\mathrm{HI}) \sim 10^{21}$ cm^{-2}, whereas most tidal arm material has substantially lower gas column densities. Such a column density criterion could also explain why, such as is perhaps the case for the NGC 4038/9 TDG, several "hotspots" are present but the future galaxy is not yet well-defined.

4.2. CO emission and H$_2$ formation

In our paper presenting the first CO detections in TDGs (Braine et al. 2000), Arp 105S and Arp 245N, we ascribed the CO emission to the formation of molecular gas from the HI. Below we give a more detailed justification and show problems with other possibilities.

The transformation of HI into H$_2$ occurs on dust grains at a rate of

$$R = 1/2\, \gamma\, n_{\mathrm{d}} n_{\mathrm{HI}} < v_{\mathrm{H}} > < \sigma_{\mathrm{d}} > \mathrm{H}_2 \; \mathrm{cm}^{-3}\, \mathrm{s}^{-1} \qquad (7)$$

where γ represents the fraction of hydrogen atoms landing on dust grains which form H$_2$ molecules, n_{d} and n_{HI} refer to the number densities in cm^{-3} of dust and atomic hydrogen, $< v_{\mathrm{H}} >$ is the average relative dust-gas velocity (thus roughly thermal), and $< \sigma_{\mathrm{d}} >$ is the dust cross-section. The factor $1/2$ is introduced because it takes 2 hydrogen atoms to form H$_2$. $\gamma < v_{\mathrm{H}} >$ is expected to be about 5×10^4 cm s^{-3} (see Hollenbach et al. 1971, and references therein). Assuming a standard distribution of dust grain sizes (Mathis et al. 1977) from 100 Å to 0.3 μm with $\frac{\mathrm{d}N(a)}{\mathrm{d}a} \propto a^{-3.5}$ where a is the grain radius and grains are assumed spherical, a gas-to-dust mass ratio of 140 (equivalent to 100 when He is disregarded), and a grain density of 2 g cm^{-3}, we obtain $n_{\mathrm{d}} < \sigma_{\mathrm{d}} > \approx 1.4 \times 10^{-20}\; n_{\mathrm{H}}$ cm^2 where $n_{\mathrm{H}} = n_{\mathrm{HI}} + 2n_{\mathrm{H}_2}$. The value is sensitive to the lower limit in dust size; allowing smaller dust grains results in even higher cross-sections or, put differently, increasing the lower bound on the grain size spectrum decreases the effective dust cross-section such that the rate is lower. Since we are interested in the start of the HI $\rightarrow$ H$_2$ conversion process, the gas can be considered to be atomic such that $n_{\mathrm{H}} \approx n_{\mathrm{HI}}$. Substituting into the above equation, one finds $R \approx 3.5 \times 10^{-16}\; n_{\mathrm{HI}}^2$ cm^{-3} s^{-1} where n is in cm^{-3}. The corresponding time to transform 20% of the atomic hydrogen into H$_2$ is $t_{20\%} \approx \frac{10^7}{n_{\mathrm{HI}}}$ years. In the outer regions of spiral galaxies the gas-to-dust mass ratio may be somewhat lower, reducing the number of H-grain collisions, but calculations with non-spherical grains will

Fig. 8. (*Top*): comparison of gas consumption time, M_{mol}/SFR, which is the inverse of the frequently used Star Formation Efficiency (SFE), as a function of blue luminosity for the different categories of galaxies. Small filled triangles represent the TDGs (data from Tables 2 and 5), open triangles the regular dwarf galaxies (data from Table 4), and the star an average spiral as taken from Kennicutt (1998), similar in position on the diagram to the Milky Way. For Arp 245N values are for the CO-detected area, not just the center. The smaller stars give the range for "average" spirals. (*Middle*): as above but as a function of oxygen abundance. (*Bottom*): molecular to atomic gas mass ratios as a function of oxygen abundance. NGC 4214 has been moved slightly to the right to make it visible and the up arrow is because the HI mass is for a substantially greater area than covered by the CO observations. The same $N(\mathrm{H}_2)/I_{\mathrm{CO}}$ value has been used for all galaxies, irrespective of metallicity or other influences, so M_{mol} is likely underestimated by a varying factor for the non-TDG dwarf galaxies.

Table 4. From our assessment of the literature, this is the entire sample of dwarf galaxies with reliable published detections both in CO and Hα. Distances are from Mateo (1998) for local group galaxies, from Israel (1988) for NGC 1569, and from Hunter et al. (1993) for NGC 4214 and NGC 4449. Except for the LMC and SMC, Hα data are from Hunter et al. (1993) and blue luminosities are from RC3 (de Vaucouleurs et al. 1991). The Hα data from Hunter et al. (1993) has been corrected for Galactic extinction. We have looked through the ensemble of CO observations of these systems. In general, IRAM 30 meter data were preferred, followed by SEST 15 m and then the NRAO 12 m. The total fluxes (or H$_2$ masses, taking into account the $N(H_2)/I_{CO}$ factor used by the authors) were converted into Jy km s^{-1} and then H$_2$ mass as explained in Sect. 2. The HI masses refer – where such an estimate was possible – to roughly the areas for which CO was measured. All values have been recalculated when necessary using the distances in Col. 2.

Galaxy	Dist. Mpc	metallicity log(O/H)+12	S_{co} Jy km s^{-1}	$L_{H\alpha}$ 10^{39} erg s^{-1}	M_{mol} 10^6 $M_\odot$	L_B 10^8 $L_{B,\odot}$	M_{HI} 10^8 $M_\odot$
LMC	0.049	8.4[2]		26[11]	13[1]	21[3]	3.3[1]
SMC	0.058	8.0[2]		4.0[11]	1.2[4]	4.9[5]	4.3[4]
IC 10	0.825	8.2[16]		11	3[6]	5.7	1.5[12]
NGC 6822	0.49	8.2[16]	121[7]	3.7	0.3	1.6	0.6[13]
NGC 1569	2.2	8.2[17]	23[8]	48	1.2	12	0.7[14]
NGC 4214	5.4	8.2[18, 19]	31[9]	26	9.7	40	19[15]
NGC 4449	5.4	8.6[19, 20]	280[10]	71	88	47	9[10]

References are: 1 = Cohen et al. (1988) find 1.4×10^8 $M_\odot$ of molecular gas assuming $M(He) = 0.4\, M(H_2)$, $N(H_2)/I_{CO} = 1.68 \times 10^{21}$ and $D = 55$ kpc, such that $M(H_2)$ with our distance and conversion factor is $10^8 \times (49/55)^2 \times 2/16.8 = 9.45 \times 10^6$ $M_\odot$. With our He fraction, this becomes $M_{mol} = 1.3 \times 10^7$ $M_\odot$. M_{HI} derived by taking the rough H$_2$/HI ratio of 30% given by Cohen et al. (1988) and their H$_2$ mass of 10^8 $M_\odot$; 2 = Dufour et al. (1982); 3 = de Vaucouleurs & Freeman (1972); 4 = Rubio et al. (1991) find $M(H_2) = 3 \times 10^7$ $M_\odot$ with $N(H_2)/I_{CO} = 6 \times 10^{21}$ and $D = 63$ kpc. Working backwards, $M_{mol} = 0.73^{-1} (58/63)^2\, 2/60 \times 3 \times 10^7$ $M_\odot = 1.16 \times 10^6$ $M_\odot$. M_{HI} derived by taking the rough H$_2$/HI ratio of 7% given by Rubio et al. (1991) and their H$_2$ mass of $3 \times 10^7 M_\odot$; 5 = Bothun & Thompson (1988); 6 = Becker (1990); 7 = Israel (1997a) sum 15 positions observed with the SEST and find $I_{CO} = 6.4 \pm 1.2$ K km s^{-1} on the main beam scale, yielding 121 Jy km s^{-1}. They note that the total CO emission of NGC 6822 may be about twice this; 8 = Taylor et al. (1998) find $I_{CO} = 0.655$ K km s^{-1} on the T_R^* scale or 23 Jy km s^{-1} for the cited 34 Jy/K efficiency; 9 = Taylor et al. (1998) find $I_{CO} = 0.9$ K km s^{-1} on the T_R^* scale, yielding 31 Jy km s^{-1}; 10 = We estimate that the sum of the CO emission observed by Hunter et al. 2000 and Hunter & Thronson (1996) corresponds to about 280 K km s^{-1} (4.2 K km s^{-1} by summing the eight positions in Table 1 of Hunter & Thronson 1996 at 34 Jy/K and about the same for the non-redundant positions in Hunter et al. 2000). The HI mass was determined for the same area, such that the CO/HI ratio is an upper limit because HI was detected in several positions where CO was not; 11 = Kennicutt et al. (1995), who take distances of 50 and 60 kpc for the LMC and SMC respectively; data not corrected for galactic extinction; 12 = Huchtmeier & Richter (1986). 13 = estimated from Gottesman & Weliachew (1977), for a region about 6' by 6'; 14 = Stil & Israel (priv. comm.). 15 = Melisse & Israel (1994), their source 71 of Sm sample, corrected for our assumed distance but covers a much larger area than the CO observations; 16 = Mateo (1998); 17 = Kobulnicky & Skillman (1997); 18 = Kobulnicky & Skillman (1996); 19 = Hunter et al. (1982), who find 12+log(O/H) = 8.6 for NGC 4214 and NGC 4449; 20 = Talent (thesis in 1980), cited by Hunter & Thronson (1996), finds 12+log(O/H) = 8.3 for NGC 4449.

tend to produce higher dust cross-sections. The most sensitive parameter is the size of small dust grains.

$t_{20\%}$ is an appropriate indicator because most of the HI gas is still in atomic form, with 20% being a typical H$_2$ fraction. The HI will become molecular in the densest parts, staying atomic in less dense regions. The timescale for the HI $\rightarrow$ H$_2$ conversion is thus much shorter than the other galaxy interaction and formation timescales, of order Myr for typical densities (after some contraction) of $n_H \gtrsim 10$ cm^{-3}. The HI $\rightarrow$ H$_2$ conversion is thus not able to slow down the gravitational collapse.

The average HI column density is probably not very relevant in and of itself. Rather, once the surrounding material is gravitationally contracting, the HI clouds come closer together and provoke the transformation of HI

into H$_2$, which is what allows star formation to proceed. This is what we see in the TDGs. An interesting counterexample is the western tidal arm (or tail) of NGC 2782. It clearly stems from NGC 2782 and is very HI-rich with many condensations with average column densities of $N_{HI} \sim 10^{21}$ cm^{-2} over regions several kpc in size (Table 4 of Smith 1994). The HI is accompanied by a weak cospatial stellar plume of surface brightness about $\mu_B \sim 25$ (Smith 1991) or perhaps slightly weaker (from comparison with Jogee et al. 1998). Neither we nor Smith et al. (1999) detected CO despite the high HI column densities and the presence of disk stars.

NGC 2782 has no single big (TDG-sized) HI condensation at the end of the western tidal tail and indeed the lack of CO provides a coherent picture: the HI here is not

condensing because the tail is not gravitationally bound and thus H_2 is not forming so star formation has not started. In fact, the interaction has certainly added some energy to the tail so we expect that the clouds may separate further. In the cases where CO is detected, the large (TDG) scale is gravitationally bound and even though large amounts of H_2 do not form in the outer disks of spirals, H_2 forms here because the HI clouds become closer to each other with time, pushing them to form H_2. At any rate, the western tail of NGC 2782 is straightforward observational evidence that CO is *not* brought out of spiral disks.

4.3. Evolution and morphology

Assuming TDGs are not short-lived objects, they condense from the tidal tail, the unbound parts of which slowly separate from the TDG. TDGs can then be arranged in a morphological evolutionary sequence which follows (*a*) their degree of detachment from the tidal tail, which can be roughly defined as the density enhancement with respect to the tidal tail, and (*b*) the compactness of the object, which is a measure of the degree of condensation of the gas (stars are non-dissipative so the old stellar population, if present, will not "condense"). The classification (evolved, intermediate, young) is simple for a number of objects. Arp 105S is clearly very compact and, at the opposite end, NGC 4038S and NGC 4676N are only just condensing from the tidal tail, being non-compact and with only a small density (light or HI) enhancement with respect to the tail. NGC 7252W is clearly more enhanced and compact than either NGC 4038S or NGC 4676N but nothing like Arp 105S. The same is true for the much more massive Arp 245N. For the NGC 5291 TDGs the stellar enhancement is total and the HI enhanced by a factor of a few, although it is still extended; they are clearly more evolved by these criteria than Arp 245N. NGC 7319E is not currently classifiable because we do not know whether it belongs to an extended optical structure or not. The sequence represents evolution, not necessarily age; simulations show, for example, that the NGC 7252 merger is much older than the Arp 245 interaction (Hibbard & Mihos 1995; Duc et al. 2000).

The conversion of HI into H_2 during contraction suggests that the H_2 to HI mass ratio may also be a tracer of evolutionary state. While a real starburst may blow the gas out of a small galaxy, the $H\alpha$ luminosities do not suggest that this is the case for the TDGs here. In Fig. 9 we plot the molecular-to-atomic gas mass ratio as a function of class, where increasing class indicates less evolved objects. Within the criteria defined in the preceding paragraph, objects can be moved around somewhat but the main subjectivity is where the NGC 5291 TDGs are placed between Arp 105S and Arp 245N, showing in all cases that the two evolutionary tracers behave in a similar fashion. That no known objects occupy the up-

per right part of the figure is further evidence that the H_2 (or CO) does not come from pre-existing clouds in spiral disks but rather formed in a contracting object. New high-resolution VLA HI and Fabry-Perot $H\alpha$ data should allow subtraction of the tail contribution and enable dynamical, and not purely morphological, criteria to be taken into account (work in progress). We will then be able to check and quantify the qualitative evolutionary sequence proposed here.

4.4. Other scenarios

In the disks of spiral galaxies, the HI emission is typically very extended, reaching 1.5–3 times the optical radius, whereas the CO emission is from well within the optical disk. At the scales sampled by the CO and HI observations, 1–10 kpc, the CO is detected at the HI column density peak and shares (see spectra) the same kinematics in terms of observed line velocity and width. In this context, given the greatly differing CO and HI emission distributions in spiral galaxies, the molecular gas which we detect has not come from the CO-rich inner parts of the parent spiral disks. The other possibilities are that (1) diffuse molecular gas containing CO but not detected in emission in spirals is present in the outer disk and that this gas is projected out of the spiral with the HI and some stars and becomes denser as the TDG forms, becoming visible in CO; or (2) that very low-metallicity H_2 is present in the outer disks of spirals (Pfenniger et al. 1994) in large quantities (Pfenniger & Combes 1994) and, once in the TDG, forms stars and the CO is detected only after sufficient enrichment of the gas.

4.4.1. Diffuse molecular gas from parent spirals

The CO brightness of galaxies decreases strongly at large galactocentric radii to the point that CO emission is not detected at or beyond the optical radii of external galaxies (García-Burillo et al. 1992; Neininger et al. 1996; Braine et al. 1997). Could there be a substantial reservoir of diffuse molecular gas present at large radii but nearly undetectable in emission?

At CO column densities of a few 10^{14} cm^{-2}, CO becomes self-shielding and starts to approach its normal abundance in molecular clouds (Liszt & Lucas 1998). This corresponds to typical H_2 column densities of several 10^{20} cm^{-2}. Depending on the size (i.e. density) of the cloud, this is close to the atomic – molecular gas transition. From absorption measurements toward stars, when the total hydrogen column density $(N_H + 2N_{H_2})$ is of order a few 10^{20} cm^{-2} or less, the molecular hydrogen fraction is very small (Federman et al. 1979). This means that if the gas is dense enough to form molecular clouds, it is also dense enough to have a normal CO content. *The molecular*
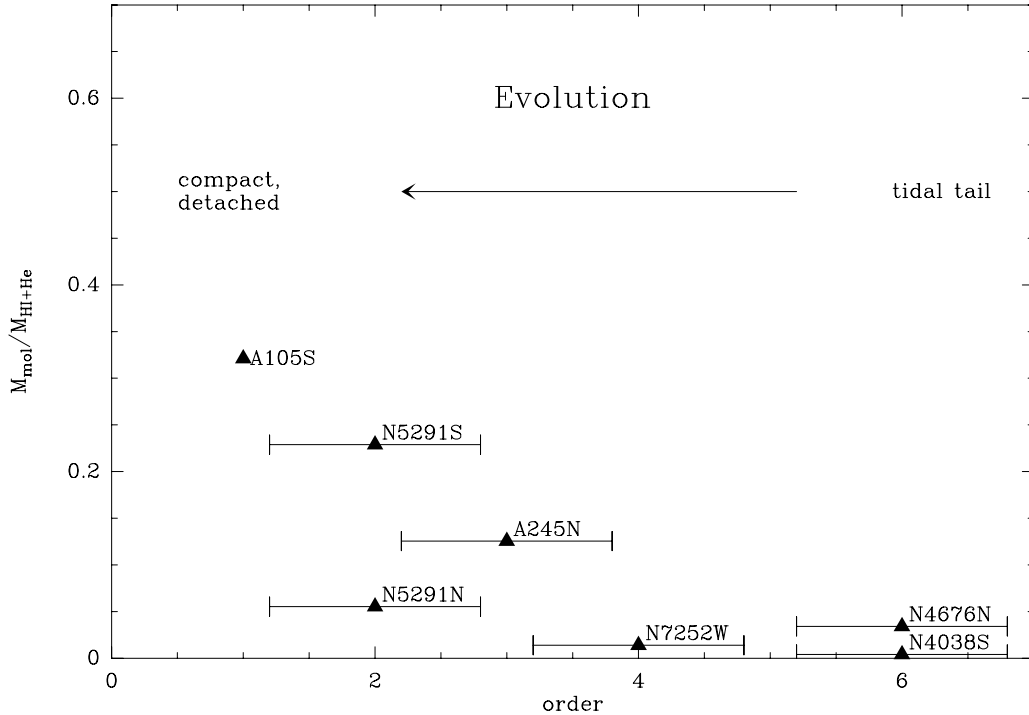
Fig. 9. Comparison of the H_2/HI mass ratio with the evolutionary order of the TDGs. NGC 7319E was not included due to its unclear morphology (see Fig. 6). The single non-detection, IC 1182E, was also left out. The errorbars indicate the uncertainty in the evolutionary order based on the criteria described in the text. The source names are to the right of their positions.

gas we observe in TDGs is not drawn from pre-collision diffuse molecular gas.

The observations of molecules, particularly CO, in emission and absorption towards quasars by Liszt & Lucas (1998 and earlier) have shown that CO is detected in emission in virtually all cases. This shows that there is not a substantial population of molecular clouds in the Galaxy where the CO is present but too cold ($T \lesssim 6$ K) to be detected in emission. The CO emission in TDGs therefore does not come from cold molecular clouds heated through the collision. We have no cases of clouds capable of hiding a substantial molecular gas mass through low CO emission.

Molecular gas detected by UV absorption in the Galactic thick disk (or lower halo) at roughly the solar circle has extremely low column densities and high ionization fractions (e.g. Richter et al. 2001). It clearly cannot play a role here.

It has been suggested that in low-metallicity environments like the LMC diffuse H_2 could be present without CO (in emission or absorption), which would be photodissociated (Israel 1997b). The lower metallicity would allow H_2 to become self-shielding at lower column densities than the CO. A similar picture was proposed by Madden et al. (1997) to explain the CII intensities observed in IC 10. Such schemes may be realistic in strong radiation fields, where small dense CO-emitting clumps are surrounded by larger masses of diffuse molecular gas

in which CO is photodissociated, but certainly not in the outer parts of a spiral galaxy. In the low ambient radiation fields in the outer parts of spirals there is no indication that CO emission is from a reduced portion of the molecular cloud. This can be simply seen as the competition between the metallicity gradient in spiral disks, of order 0.2 dex per disk scale length (see Table 3 of Zaritsky et al. 1994) and the brightness gradient, 0.43 dex per disk scale length. Only when the metallicity decreases by close to an order of magnitude such that the CO(1–0) line becomes optically thin will H_2 be efficiently hidden from CO observations in spiral disks (Wolfire et al. 1993; Braine et al. 1997).

4.4.2. Rapid enrichment of molecular gas through star formation

Star formation is occuring in many dwarf galaxies of sizes comparable to TDGs (Taylor et al. 1998; Hunter et al. 1993) at rates at least as high as in our TDG sample. Were star formation capable of enriching gas sufficiently to render the CO emission as strong as in TDGs, many blue dwarf galaxies would emit very strong CO lines. As examples, NGC 1569 and NGC 4449 have star formation rates of about 0.6 and 0.9 $M_\odot$ yr^{-1} (Table 4, Eq. (5)) and have presumably been forming stars for a period at

least as long as in the TDGs yet their metallicities and CO luminosities are substantially lower than in TDGs.

CO is detected in the M 81 group tidal debris (in IMC, Brouillet et al. 1992), where no star formation nor detected old stellar population is present so clearly no post-interaction enrichment has taken place. This is confirmed by the presence of detectable ^{13}CO in IMC1 (work in progress) which is chiefly synthesized in evolved stars of intermediate masses (Wheeler et al. 1989). That TDGs share a roughly common metallicity (Duc et al. 2000) regardless of luminosity suggests that the material is globally enriched such that as the post-interaction star formation is inefficient at increasing the metallicity, the metallicity stays at its original spiral-disk level.

5. CO linewidths and Tidal Dwarf Galaxy masses

While data are still sparse, we believe there is a correlation between CO line widths and mass indicators. Because CO is found in the condensed parts of TDGs, it is a better mass indicator than the HI linewidth, for which the contribution of the tidal tails or other unbound material (not TDG) cannot be easily assessed. Clearly, a regular HI (or CO) rotation curve would be extremely useful and convincing as a measure of mass. So far, regular rotation curves have not been observed in TDGs although velocity gradients, possibly rotation, in the ionized gas have been detected (Duc & Mirabel 1998).

In order to trace the mass of a system, the material used as a tracer must be (*a*) gravitationally bound and (*b*) roughly as extended (or more) as the mass distribution. We believe that CO fulfills these conditions for TDGs. The fact that the CO is found where the HI column density is high, and that it formed from the condensation of the HI, is good evidence for condition *a*. The second condition is more problematic given the large distance and small angular size of most of our sources but nonetheless several considerations lead us to think it is justified. The only extended TDGs, with respect to the resolution of our observations, are NGC 4038S and Arp 245N. Arp 245N is roughly as extended in CO as at other wavelengths; NGC 4038S was only observed at one position. No abundance gradient has been detected or is expected in current TDGs so one may reasonably expect CO to be visible wherever HI has condensed into H_2. Many dwarf galaxies have very extended HI distributions, up to several times the size of their optical extent. In TDGs, the evidence points to relatively co-spatial dense gas and old stellar populations although the relative distributions in the parent disk and collision parameters condition the mass ratio. The diffuse, unbound, HI in tidal tails is unlikely to form H_2 so the molecular component should yield a complete but less confused picture of the dynamics. Possibly for the reason suggested in Sect. 6, dwarf galaxies have rather dense dark matter (DM) haloes, such that they have a discernible dynamical influence even within the

Table 5. CO linewidths of detected TDGs. ΔV is full width at half maximum. R (Col. 4) is half the CO beamsize except for Arp 245N where R is estimated to be $27''$ and NGC 4676N where R is taken to be $21''$ (half the extent of the observed region). NGC 4676N is still a tidal tail and the L_B and $M(HI)$ values are for the whole North tail. The : indicates an uncertain value – both the CO(2–1) and HI line widths are lower than the CO(1–0) width for NGC 5291N.

TDG	ΔV_{CO}	Luminosity	$R\Delta V^2/G$	M_{HI}
	$km\,s^{-1}$	$10^8\,L_{B,\odot}$	$10^8\,M_\odot$	$10^8\,M_\odot$
Arp 105S	35	9.0^a	17	5^b
Arp 245N	49	9.2^c	22.6	9^c
NGC 7252W	12	1.2^d	0.6	$10{:}^e$
NGC 4038S	8	0.8^f	0.1	3^g
NGC 5291N	130:	4.7^h	243	25^i
NGC 5291S	70	2.2^h	70	9^i
NGC 7319E	30	1.0^j	10	9^k
NGC 4676N	45	66^l	43	22^m

References: *a*: Duc & Mirabel (1994); *b*: Duc et al. (1997); *c*: Duc et al. (2000); *d*: Duc (1995); *e*: estimated from Hibbard et al. (1994); *f*: estimated from Mirabel et al. (1992) using $B - V = 0.2$ as for both NGC 7252 TDGs; *g*: estimated from van der Hulst (1979); *h*: Duc & Mirabel (1998); *i*: Duc & Mirabel (1998); estimated from Malphrus et al. (1997); *j*: Xu et al. (1999); *k*: estimated from Shostak et al. (1984); *l*: this paper; *m*: estimated from Hibbard & van Gorkom (1996).

optically bright regions (Côté et al. 2000). The old stellar population of TDGs varies greatly but is in general quite dim, furthering the expectation that were DM present in TDGs, we would see it in the gas dynamics.

In Table 5 we give the line widths of the detected TDGs, their blue luminosities, the so-called "Virial masses" $M_{vir} \approx R\Delta V^2/G$, and HI masses and the same are plotted in Fig. 10. The apparent, although very rough, correlation is an indication that the line widths are indeed related to mass, analogous to the Tully-Fisher relation for spirals. We infer this principally from the unpopulated lower right (high mass, low linewidth) and upper left (low mass, high linewidth) corners of the panels. In turn, this implies that (*a*) the objects are kinematically distinct from the parent galaxies and (*b*) the linewidths can be used as an indicator of mass. We say indicator of mass as opposed to measure of mass because of the great uncertainties, factor 2 or more, in the geometry as well as in the degree of relaxation of the objects. The uncertainty is not symmetric, however, as lines can be widened more easily than narrowed. Low values of $R\Delta V^2/M_\odot G$ are thus significant.

Figure 10 shows the variation of the "Virial mass" with total gas mass, molecular gas mass, Blue luminosity, and our best estimate of the total mass. Tidal features are not a homogeneous class – some have virtually no pre-existing stellar component (e.g. NGC 5291N) while others (e.g.
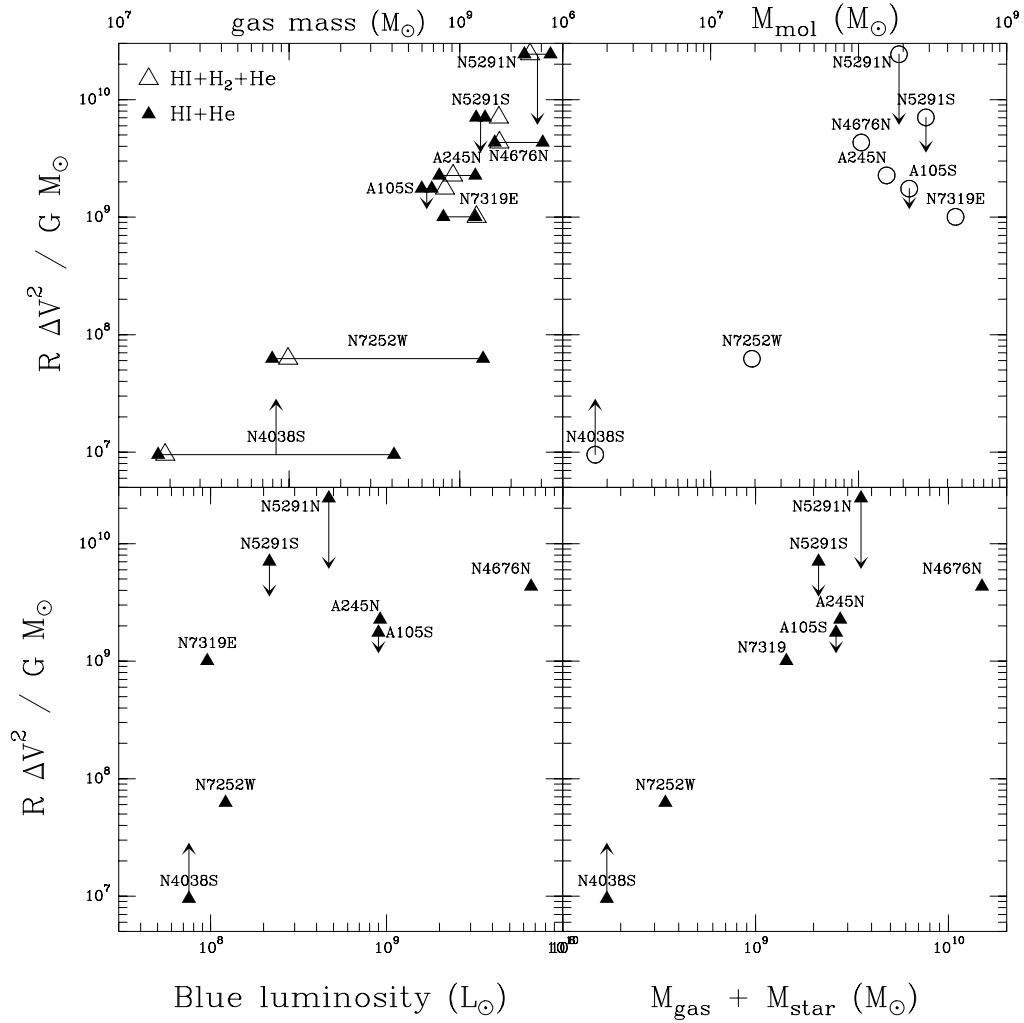
Fig. 10. Virial masses derived from CO line widths as a function of HI and total gas mass (top left), H$_2$ mass (top right), Blue luminosity (lower left), and a combination of all of the above. Ordinate axis expresses the Virial masses as $R\Delta V^2/G$. In the first panel the dark triangles joined by a line represent the HI masses within the area observed in CO and total HI masses. Open triangles give total gas masses within the CO beam(s) – these are dominated by the HI. An idea of the uncertainty and whether the value is an overestimate or underestimate is given by the presence of arrow. A downward arrow is caused by a beam which is large compared to the source size – such that $R_{\rm TDG} < R_{\rm beam}$ (Arp 105S, NGC 5291S, NGC 5291N) – or that ΔV is likely an overestimate (NGC 5291N). NGC 4038S is larger than the beam but only one position was measured – hence the up arrow. The position of the end of the arrow is our best estimate, based on source size or line widths in other lines, of where the point should really be placed in the figure.

Arp 245N) have a significant contribution from disk stars. To take this into account, we tried to sum the masses of the gaseous and stellar components in the last panel and indeed the trend shows a smaller dispersion. Although the mass to light ratio, M/L_B, certainly varies within the sample we chose a ratio of $M/L_B = 2M/L_{B,\odot}$, midway between that of young and evolved stellar populations.

The "Virial masses" of the sample span a larger range than the gas + star masses. Some of this may be due to the uncertain line width of NGC 5291N. Given the uncertainties in line widths and geometry it is too early to make definite statements but so far no dark matter is required to explain the observed CO line widths. It will

be interesting to see whether this remains true when more objects and more precise measurements are available.

If indeed TDGs do not contain DM, then
– they are the only DM-free galaxies identified so far;
– DM is found in the haloes of spiral galaxies;
– TDGs are not representative of the population of Dwarf Galaxies with measured rotation curves as these are quite DM-rich.

6. Conclusions

We report the second series of CO detections in Tidal Dwarf Galaxies, raising the number of detections from two to eight and showing that molecular gas is abundant in

these objects. The molecular gas is formed from the condensing atomic gas, which in turn condenses to form stars, responsible for the Hα emission observed. The CO/Hα flux ratio, akin to a gas consumption time, is much higher than in "standard" dwarf galaxies and about the same as what is found in spiral galaxies despite the very different environments.

A correlation is present between the dynamical masses, determined from the sizes and CO line widths, and mass estimators like HI mass and optical luminosity. In addition to the fact that CO is found where the HI column density is high, and thus most likely to be gravitationally bound, the mass-linewidth correlation reinforces the idea that the CO emission comes from a gravitationally bound entity. Comparing the dynamical masses with estimates of the gas+stellar mass reveals no need for dark matter. The uncertainties linked to the small sizes of the objects, observational noise, and particularly the unknown geometry, do not enable us to firmly exclude the presence of dark matter, although with the current sample of eight objects it appears increasingly unlikely that large quantities of DM are present. Large quantities of DM are not expected to be present in TDGs if the DM in spiral galaxies is found in haloes.

Our tentative conclusion that TDGs contain little or no dark matter strongly implies that most dwarf galaxies are *not* old TDGs. This can be understood in the CDM hierarchical structure formation framework (e.g., White & Rees 1978; Kauffmann et al. 1993) where concentrations merge to form larger and larger systems, becoming full-fledged galaxies. This process continues to the present but collisions become much less frequent with time due to the decreasing galaxy density (expansion of the universe). Non-tidal dwarf galaxies formed on average at higher redshift in this picture and thus have more concentrated dark matter haloes than spirals. Hierarchical clustering thus reproduces an important observation: that larger galaxies require less dark matter within the optically visible part (Casertano & van Gorkom 1991). Our results fit into this picture.

Appendix A: other cases of molecular gas outside of spiral disks

Several examples of molecular gas being detected in "non-traditional" places have been reported in the literature. We describe them briefly below.

M 81 – IMC 1 & 2: The first intergalactic molecular clouds (hence the name IMC) were discovered by Brouillet et al. (1992) as part of the M 81 group tidal material. So far, no stellar emission has been detected from this object (Henkel et al. 1993). A similar object was recently found by Walter & Heithausen (1999) near NGC 3077 in the same group, again with no sign of a stellar component. These objects may well be small "future TDGs", using the definition of a TDG as containing a stellar component. Like our sources, the molecular gas is found at the HI column density peak and must have formed from the atomic gas.

NGC 4438: In this HI poor galaxy near the center of the Virgo cluster Combes et al. (1988) detected large quantities of molecular gas significantly out of the plane of the spiral disk. They suggest the material was torn out of the disk in molecular form, along with some stars, through an interaction with nearby NGC 4435. Little HI is present so HI → H$_2$ conversion appears very unlikely.

NGC 660: Combes et al. (1992) detected CO in the polar ring near the HI maxima. Given the size of the ring, the CO is likely to have been formed from the HI. Nonetheless, the result of a major fusion, producing a polar ring, is a rather confused object so we chose not to include it in our sample.

NGC 2782 (Arp 215): Smith et al. (1999) detected CO in what appears to be the base of the eastern tidal tail. The tail seems dynamically separate from the main galaxy but interpretation of the CO emission requires much higher angular resolution.

NGC 5128 (Centaurus A): Molecular gas was recently detected by Charmandaris et al. (2000) in the gaseous shells of Centaurus A, a galaxy which also contains several stellar shells. It is widely accepted that the formation mechanism for stellar shells can result from a minor merger (Quinn 1984; Dupraz & Combes 1987) while the details of the dynamical behavior of the gaseous component in minor mergers is still an open issue. Since TDGs seem to form as a result of major interactions/mergers and Centaurus A is a rather unique object so far, we do not include it in our sample.

UGC 12914/5: We have mapped CO(1–0) and CO(2–1) in the bridge linking the two spirals (work in progress). Given the collision (Condon et al. 1993; Jarrett et al. 1999), it is quite possible the molecular gas was taken out of the inner parts of the spiral(s) in molecular form, closer to the situation in NGC 4438 than in TDGs.

Table B.1. CO(1–0) fluxes and estimated molecular gas masses in the centers of the observed systems. The actual spectra are shown in the figures given in Col. 5. The galaxy classification (morphological type in Col. 2) is only a rough indication of their properties given the changes induced by the tidal forces. The first type given comes from the RC3 catalog (de Vaucouleurs et al. 1991) and the others from the references below. NGC 7252 was also observed at lower resolution by Dupraz et al. (1990). For IC 1182, as this object is resolved, we give first the central flux and M_{mol} followed by our estimate of the total based on the CO spectra shown in the figure.

Galaxy	type	S_{CO}	M_{mol}	Fig.
		Jy km s^{-1}	$10^9\ M_\odot$	
NGC 2992	Sa, Sa?[a]	137	1.4	3
NGC 2993	Sa, Sa?[a]	132	1.4	3
NGC 5291	E, E?[a]	48	1.7	2
NGC 4676a	S0, Sa[b]	59	5.1	5
NGC 7252	S0, E-S0[a]	82	3.6	3
IC 1182	S0-a	25, 35	5, 7	7

[a] Prugniel & Héraudeau (1998); [b] Karachentsev (1987).

Appendix B: Molecular gas in the galactic centers

To our knowledge no CO observations of the main galaxies in several of these systems has been published and in others only lower resolution data is available. The same fairly standard factor $N(H_2)/I_{CO(1-0)} = 2 \times 10^{20}\ cm^{-2}\,(K\,km\,s^{-1})^{-1}$ has been used as for the TDGs. We give CO(1–0) fluxes and estimated molecular gas masses for the central $22''$ of these galaxies in Table B.1. All spectra are shown in the figures whose numbers are in Col. 5.

References

Arnault, P., Kunth, D., Casoli, F., & Combes, F. 1988, A&A, 205, 41

Barnes, J. E., & Hernquist, L. 1992, Nature, 360, 715

Becker, R. 1990, Ph.D. Thesis, University of Bonn, Germany

Blumenthal, G. R., Faber, S. M., Primack, J. R., & Rees, M. J. 1984, Nature, 311, 517

Bothun, G. D., Stauffer, J. R., & Schommer, R. A. 1981, ApJ, 247, 42

Bothun, G. D., & Thompson, I. B. 1988, AJ, 96, 877

Braine, J., Brouillet, N., & Baudry, A. 1997, A&A, 318, 19

Braine, J., Lisenfeld, U., Duc, P.-A., & Leon, S. 2000, Nature, 403, 867

Brouillet, N., Henkel, C., & Baudry, A. 1992, A&A, 262, L5

Casertano, S., & van Gorkom, J. H. 1991, AJ, 101, 1231

Charmandaris, V., Combes, F., & van der Hulst, J. M. 2000, A&A, 356, L1

Cohen, R. S., Dame, T. M., Garay, G., Rubio, M., & Montani, J. 1988, ApJ, 331, L95

Combes, F., Braine, J., Casoli, F., Gerin, M., & van Driel, W. 1992, A&A, 259, L65

Combes, F., Dupraz, C., Casoli, F., & Pagani, L. 1988, A&A, 203, 9

Condon, J. J., Helou, G., Sanders, D. B., & Soifer, B. T. 1993, AJ, 105, 1730

Côté, S., Carignan, C., & Freeman, K. C. 2000, AJ, 120, 3027

de Vaucouleurs, G., de Vaucouleurs, A., Corwin, J. R., et al. 1991, in Third reference catalogue of bright galaxies

de Vaucouleurs, G., & Freeman, K. C. 1972, Vistas Astron., 14, 163

Dickey, J. M. 1997, AJ, 113, 1939

Dickman, R. L., Snell, R. L., & Schloerb, F. P. 1986, ApJ, 309, 326

Duc, P.-A. 1995, Ph.D. Thesis, Université Paris VI

Duc, P.-A., Brinks, E., Springel, V., et al. 2000, AJ, 120, 1238

Duc, P.-A., Brinks, E., Wink, J. E., & Mirabel, I. F. 1997, A&A, 326, 537

Duc, P.-A., & Mirabel, I. F. 1994, A&A, 289, 83

Duc, P.-A., & Mirabel, I. F. 1998, A&A, 333, 813

Dufour, R. J., Shields, G. A., & Talbot, R. J. 1982, ApJ, 252, 461

Dupraz, C., Casoli, F., Combes, F., & Kazes, I. 1990, A&A, 228, L5

Dupraz, C., & Combes, F. 1987, A&A, 185, L1

Federman, S. R., Glassgold, A. E., & Kwan, J. 1979, ApJ, 227, 466

Gallagher, S. C., Charlton, J. C., Hunsberger, S. D., Zaritsky, D., & Whitmore, B. C. 2001, AJ, 122, 163

Gao, Y., Lo, K., Lee, S.-W., & Lee, T.-H. 2001, ApJ, 548, 172

García-Burillo, S., Guélin, M., Cernicharo, J., & Dahlem, M. 1992, A&A, 266, 21

Gottesman, S. T., & Weliachew, L. 1977, A&A, 61, 523

Henkel, C., Stickel, M., Salzer, J. J., et al. 1993, A&A, 273, L15

Hibbard, J. E., Guhathakurta, P., van Gorkom, J. H., & Schweizer, F. 1994, AJ, 107, 67

Hibbard, J. E., & Mihos, J. C. 1995, AJ, 110, 140

Hibbard, J. E., & van Gorkom, J. H. 1996, AJ, 111, 655

Hickson, P. 1982, ApJ, 255, 382

Hollenbach, D. J., Werner, M. W., & Salpeter, E. E. 1971, ApJ, 163, 165

Huchtmeier, W. K., & Richter, O. G. 1986, A&AS, 63, 323

Hunter, D. A., & Gallagher, J. S. 1986, PASP, 98, 5

Hunter, D. A., Gallagher, J. S., & Rautenkranz, D. 1982, ApJS, 49, 53

Hunter, D. A., Hawley, W. N., & Gallagher, J. S. 1993, AJ, 106, 1797

Hunter, D. A., & Thronson, H. A. 1996, ApJ, 461, 202

Hunter, D. A., Walker, C. E., & Wilcots, E. M. 2000, AJ, 119, 668

Israel, F. P. 1988, A&A, 194, 24

Israel, F. P. 1997a, A&A, 317, 65

Israel, F. P. 1997b, A&A, 328, 471

Jarrett, T. H., Helou, G., Van Buren, D., Valjavec, E., & Condon, J. J. 1999, AJ, 118, 2132

Jogee, S., Kenney, J. D. P., & Smith, B. J. 1998, ApJL, 494, L185

Karachentsev, I. 1987, Moscow Izdatel Nauka

Kauffmann, G., White, S. D. M., & Guiderdoni, B. 1993, MNRAS, 264, 201

Kennicutt, R. C. 1989, ApJ, 344, 685

Kennicutt, R. C. 1998, ApJ, 498, 541

Kennicutt, R. C., Bresolin, F., Bomans, D. J., Bothun, G. D., & Thompson, I. B. 1995, AJ, 109, 594

Kobulnicky, H. A., & Skillman, E. D. 1996, ApJ, 471, 211

Kobulnicky, H. A., & Skillman, E. D. 1997, ApJ, 489, 636

Liszt, H. S., & Lucas, R. 1998, A&A, 339, 561

Lo, K. Y., Sargent, W. L. W., & Young, K. 1993, AJ, 106, 507

Madden, S. C., Poglitsch, A., Geis, N., Stacey, G. J., & Townes, C. H. 1997, ApJ, 483, 200

Malphrus, B., Simpson, C., Gottesman, S., & Hawarden, T. G. 1997, AJ, 114, 1427

Mateo, M. L. 1998, ARA&A, 36, 435

Mathis, J. S., Rumpl, W., & Nordsieck, K. H. 1977, ApJ, 217, 425

Melisse, J. P. M., & Israel, F. P. 1994, A&A, 285, 51

Mihos, J. C. 2001, ApJ [astro-ph/0011131]

Mirabel, I. F., Dottori, H., & Lutz, D. 1992, A&A, 256, L19

Neininger, N., Guelin, M., Garcia-Burillo, S., Zylka, R., & Wielebinski, R. 1996, A&A, 310, 725

Peebles, P. J. E. 1982, ApJ, 263, L1

Pfenniger, D., & Combes, F. 1994, A&A, 285, 94

Pfenniger, D., Combes, F., & Martinet, L. 1994, A&A, 285, 79

Prugniel, P., & Héraudeau, P. 1998, A&AS, 128, 299

Quinn, P. J. 1984, ApJ, 279, 596

Richter, P., Savage, B. D., Wakker, B. P., Sembach, K. R., & Kalberla, P. M. W. 2001, ApJ, 549, 281

Rubio, M., Garay, G., Montani, J., & Thaddeus, P. 1991, ApJ, 368, 173

Salpeter, E. E. 1955, ApJ, 121, 161

Schmidt, M. 1959, ApJ, 129, 243

Shostak, G. S., Allen, R. J., & Sullivan, W. T. 1984, A&A, 139, 15

Skillman, E. D., Kennicutt, R. C., & Hodge, P. W. 1989, ApJ, 347, 875

Skillman, E. D., Terlevich, R., Teuben, P. J., & van Woerden, H. 1988, A&A, 198, 33

Smith, B. J. 1991, ApJ, 378, 39

Smith, B. J. 1994, AJ, 107, 1695

Smith, B. J., Struck, C., Kenney, J. D. P., & Jogee, S. 1999, AJ, 117, 1237

Springel, V., & White, S. D. M. 1999, MNRAS, 307, 162

Sutton, E. C., Blake, G. A., Masson, C. R., & Phillips, T. G. 1985, ApJS, 58, 341

Taylor, C. L., Kobulnicky, H., & Skillman, E. D. 1998, AJ, 116, 2746

Toomre, A. 1964, ApJ, 139, 1217

Turner, B. E. 1989, ApJS, 70, 539

van der Hulst, J. M. 1979, A&A, 71, 131

Walter, F., & Heithausen, A. 1999, ApJ, 519, L69

Weilbacher, P. M., Duc, P.-A., Fritze von Alvensleben, U., Martin, P., & Fricke, K. J. 2000, A&A, 358, 819

Wheeler, J. C., Sneden, C., & Truran, J. W. 1989, ARA&A, 27, 279

White, S. D. M., & Rees, M. J. 1978, MNRAS, 183, 341

Wolfire, M. G., Hollenbach, D., & Tielens, A. G. G. M. 1993, ApJ, 402, 195

Xu, C., Sulentic, J. W., & Tuffs, R. 1999, ApJ, 512, 178

Zaritsky, D., Kennicutt, R. C., & Huchra, J. P. 1994, ApJ, 420, 87